Displacement Fields of Wood in Tension Based on Image Processing:
Part 2. Crack-Tip Displacements in Mode-I and Mixed-Mode Fracture

S. Samarasinghe and G.D. Kulasiri

Samarasinghe, S. & Kulasiri, G.D. 2000. Displacement fields of wood in tension based on image processing: Part 2. Crack-tip displacements in mode-I and mixed-mode fracture. Silva Fennica 34(3): 261–274.

Near tip displacement fields for tensile loaded cracked rubber and wood with a crack parallel-, perpendicular-to-grain, and a parallel-to-grain crack inclined 30°, 45°, and 60° to the load axis were obtained from digital image correlation (DIC). Theoretical displacements were also obtained for rubber and wood using isotropic and orthotropic fracture theory, respectively. The results showed that DIC can reveal fine details of the nature of displacements and the influences of crack tip in both rubber and wood. Experimental crack tip displacements for wood compare well with theory; particularly, when load is perpendicular-to-grain. Some anomalies were found in the tip displacements in the direction of the tracheids due to the unique nature of their behaviour not accounted for by theory. Mixed-mode crack tip displacement fields for wood clearly showed the increasing influence of crack angle on the displacements, and the displacements perpendicular to crack compared very well with theory. The displacements parallel to crack showed some variations owing to the involvement of tracheids.

Keywords digital image correlation, fracture modes, orthotropic fracture, tip displacement, wood
Authors´ address Lincoln University, Appl. Computing, Mathematics and Statistics Group, P.O. Box 84, Canterbury, New Zealand **E-mail** kulasird@tui.lincoln.ac.nz
Received 19 October 1999 **Accepted** 23 August 2000

1 Introduction

It is well established in fracture mechanics literature that the failure in cracked bodies is due to stress concentration effects at the tip of cracks. Therefore, a major theoretical effort has gone into characterising crack tip phenomena in materials. Early researchers (Westergaard 1939, Williams 1952, 1957) mathematically derived crack tip stress and displacement fields and Irwin (1957) showed that stresses and displacements near a crack tip could be described by a single parame-

ter, K, stress intensity factor. Underlying assumption in these derivations is that material is homogeneous and isotropic. Sih et al. (1965) mathematically formulated stresses and displacements near a crack tip in a remotely loaded orthotropic plate. This derivation assumes that the material is homogeneous, truly orthotropic (material symmetry coincides with geometric symmetry), and material properties in a given direction are constant. In wood however, orthotropy is cylindrical or conical, material symmetry axes and geometric symmetry axes of structural members do not coincide most of the time, and material properties are highly variable along the length and width. These theoretical issues and the importance of the knowledge of fracture in the design of wood structures prompted us to conduct a detailed study of the behaviour of cracks in wood.

The goal of this research is to study in detail displacement fields near a crack tip in tensile loaded wood plates in mode-I and mixed mode fracture using digital image correlation and make comparisons with theoretical crack tip displacement fields. Specifically, the following configurations have been studied: mode-I crack parallel-to-grain, mode-I crack perpendicular-to-grain, mode-I industrial rubber, and mixed-mode crack aligned along the grain but inclined 30°, 45°, and 60° to the direction of loading. The reason for testing rubber was to study displacement fields for a uniform isotropic material and make comparisons with the results obtained for highly variable and orthotropic wood.

2 Crack tip Displacement Fields

Westergaard (1939) and Williams (1952, 1957) derived formulae for horizontal (u) and vertical (v) displacements of a point located a distance r from the tip and angle θ from the crack plane (Fig. 1) as given in Eqs. (1) and (2).

$$u = \frac{K_I}{2\mu}\sqrt{\frac{r}{2\pi}}\,Cos(\theta/2)\quad\left[\kappa - 1 + 2Sin^2(\theta/2)\right] \quad (1)$$

$$v = \frac{K_I}{2\mu}\sqrt{\frac{r}{2\pi}}\,Sin(\theta/2)\quad\left[\kappa + 1 - 2\,Cos^2(\theta/2)\right] \quad (2)$$

where, K_I is mode-I stress intensity factor, $\kappa = 3 - 4\nu$ for plane strain, and ν is the poisson ratio.

Sih et al. (1965) extended Westergaard's (1939) approach to formulate the following displacement fields near a tip of a remotely loaded orthotropic plate in mode-I fracture:

$$u = K_I\sqrt{\frac{r}{2\pi}}\,\mathrm{Re}\left[\frac{1}{\mu_1 - \mu_2}\left(\mu_1 p_2\sqrt{Cos\theta + \mu_2 Sin\theta} - \mu_2 p_1\sqrt{Cos\theta + \mu_1 Sin\theta}\right)\right] \quad (3)$$

$$v = K_I\sqrt{\frac{r}{2\pi}}\,\mathrm{Re}\left[\frac{1}{\mu_1 - \mu_2}\left(\mu_1 q_2\sqrt{Cos\theta + \mu_2 Sin\theta} - \mu_2 q_1\sqrt{Cos\theta + \mu_1 Sin\theta}\right)\right] \quad (4)$$

Re is real component of the expression in square brackets, and μ_i, p_i, q_i are functions of material properties (E_L, E_R, E_T, ν_{LR}, ν_{LT}, ν_{RT}).

In mixed-mode fracture, crack is at an angle to load axis and therefore, both mode-I and mode-II fracture influences the tip behaviour. The horizontal (u) and vertical (v) displacements are the combined total of the separate displacement components due to the two modes as shown in Equations (5) and 6), respectively.

$$u = K_I\sqrt{\frac{r}{2\pi}}\,\mathrm{Re}\left[\frac{1}{\mu_1-\mu_2}\left(\mu_1 p_2\sqrt{Cos\theta+\mu_2 Sin\theta}-\mu_2 p_1\sqrt{Cos\theta+\mu_1 Sin\theta}\right)\right] + K_{II}\sqrt{\frac{r}{2\pi}}\,\mathrm{Re}\left[\frac{1}{\mu_1-\mu_2}\left(p_2\sqrt{Cos\theta+\mu_2 Sin\theta}-p_1\sqrt{Cos\theta+\mu_1 Sin\theta}\right)\right] \quad (5)$$

$$v = K_I\sqrt{\frac{r}{2\pi}}\,\mathrm{Re}\left[\frac{1}{\mu_1-\mu_2}\left(\mu_1 q_2\sqrt{Cos\theta+\mu_2 Sin\theta}-\mu_2 q_1\sqrt{Cos\theta+\mu_1 Sin\theta}\right)\right] + K_{II}\sqrt{\frac{r}{2\pi}}\,\mathrm{Re}\left[\frac{1}{\mu_1-\mu_2}\left(q_2\sqrt{Cos\theta+\mu_2 Sin\theta}-q_1\sqrt{Cos\theta+\mu_1 Sin\theta}\right)\right] \quad (6)$$

where, K_{II} is mode-II stress intensity factor and other parameters are the same as described previously. Details of these derivations are avoided for clarity and reader is referred to Sih et al. (1965) for a complete review.

Digital image correlation (DIC) is a non-contacting full-field displacement measuring technique that has been used in few studies to obtain displacement profiles for wood in compression and bending, and in wood joints as discussed in Part 1 of this study. Even fewer researchers have applied the method to study fracture mechanisms. Durig et al. (1991) applied the method to determine stress intensity factors for aluminium in mixed-mode fracture and McNeill et al. (1987) used it to obtain mode-I stress intensity factor for plexiglass. The authors have been using the method for crack tip displacement analysis and the determination of stress intensity factors for wood (Samarasinghe et al. 1996, Samarasinghe and Kulasiri 1998, 1999).

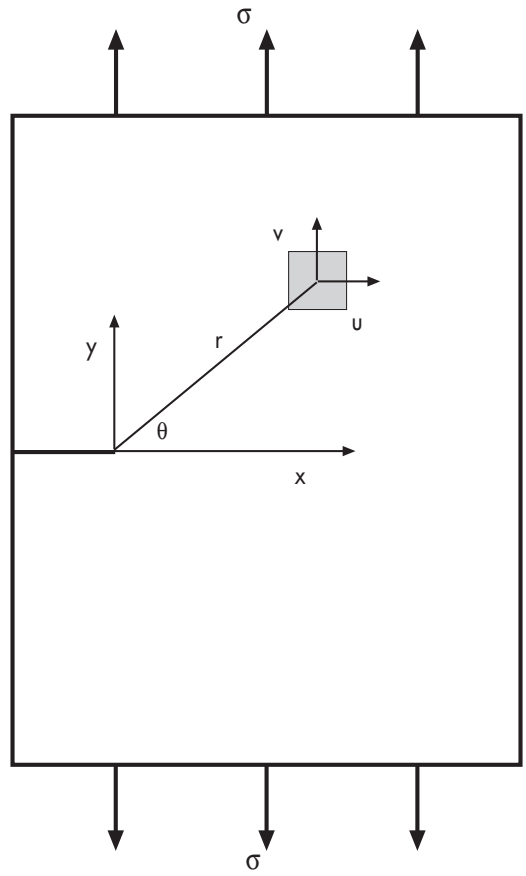

Fig. 1. Two dimensional near tip displacement components of a unit area in a plate loaded in tension.

3 Experimental Methods

Timber specimens were cut from kiln-dried flat sawn New Zealand radiata pine (*Pinus radiata*) boards obtained from a local sawmill in Christchurch, New Zealand. The boards were kept in the laboratory for seven months before they were cut into specimens whose dimensions are given in Table 1. Cracks of specified length were cut using a fine saw blade. The loading plane for wood specimens was Longitudinal-Tangential (LT) with the thickness in the radial direction. Moisture content of the specimens at the time of testing was approximately 12 %, the average density was about 400 kg/m^3, and average Young's modulus (E_L) was 8.0 GPa. Medium flexibility industrial rubber was obtained from a local shop and dimensions of the cracked rubber specimens are also shown in Table 1. Experimentally obtained Young's modulus for rubber was 3.167 MPa. All the materials used in this study were from the same batch as that used in Part 1 of the study.

Experiments were conducted on a computer controlled SINTECH/MTS material testing workstation and the testing procedure and image capture were exactly the same as that described in Part 1 of the study published along with this paper. The only difference is that the specimens in this study had an edge crack and an area near the tip was focused in image capture.

Images near the crack tip area were captured (in TIF format) and analyzed by the Video Image Correlation Program discussed in Part 1 of the study. An area of 1.0 to 2.0 cm^2 in front of the crack as shown in Figs. 2(a) and 2(b) was selected for analysis and displacements of 100 to 200 points were determined. The focus of this

Table 1. Specimen configuration and dimensions.

Specimen Configuration	Rubber	Wood crack para-to-grain	Wood crack perp-to-grain	Wood mixed-mode (30, 45, 60 angle)
Dimensions, mm (length × width × thickness)	95 × 140 × 20	230 × 140 × 20	220 × 140 × 20	180 × 90 × 20
Crack length, mm	10	20	20	12

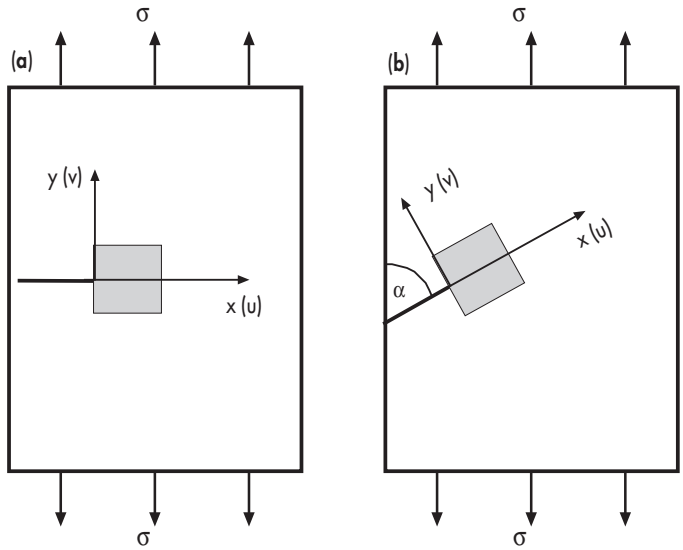

Fig. 2. Location of the analyzed area with respect to (a) Mode-I and (b) inclined cracks.

paper is on horizontal and vertical displacements as shown in Fig. 2(a) and results for a representative specimen are presented in this paper for detailed discussion and comparison between different modes.

4 Displacement Fields in the Vicinity of a Crack in Mode-I Fracture

In this section, displacement fields for a small area in front of the crack are presented for mode-I fracture in (1) rubber, (2) wood with crack parallel-to-grain, and (3) wood with crack perpendicular to grain. The location of the area analyzed is as shown in Fig. 2(a) and coordinate system is positioned such that crack tip is stationary and coincides with the origin of the coordinate system, x axis lies along the crack plane and y axis is perpendicular to the crack plane. This is the convention used in fracture mechanics theory. According to this convention crack tip does not move (v = u = 0) and the displacement of all the points are measured with respect to the tip. Further processing and plotting of the results from the digital image correlation as well as theoretical displacement profiles were done on Mathematica 3.0 (Wolfram Research 1997). The results for the isotropic rubber is presented first followed by a discussion on displacement fields for cracked wood plates.

4.1 Displacement Profiles in the Vicinity of a Crack in an Isotropic Plate

Linear elastic fracture mechanics is well established for the study of crack tip stress concentrations in isotropic materials. Therefore, it is expected that experimental displacements will resemble theoretical values. Theoretical displacement fields were obtained from Equations (1) and (2) by substituting following representative material properties: shear modulus, μ = 1.6243 MPa, Stress Intensity Factor, K_I = 0.5664 MPa$\sqrt{}$mm, and poisson ratio, ν = 0.25. The shear modulus and stress intensity factor are based on

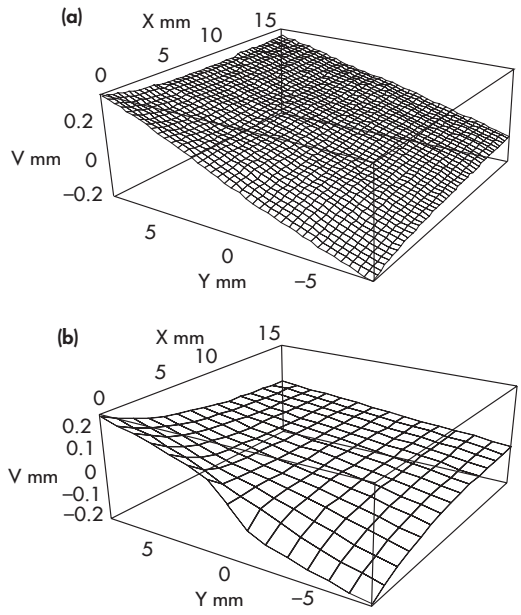

Fig. 3. Vertical displacement fields for rubber with a crack (a) experimental profile (b) theoretical profile.

the experimentally determined Young's modulus of 3.167 MPa.

A plate in the presence of a crack should deform unsymmetrically with respect to the x axis due to greater elongation of the area of the plate closer to the tip. Fig. 3(a) displays the 3-D plot for v obtained from the digital image correlation for a load of 150 N. Here the crack tip is on the front border of the plots and its coordinates are (0,0) and crack tip is stationary. What is shown is the displacement in an area of 1.75 cm × 1.58 cm in front of the crack for a total plate end extension of 3 mm. Most notable feature of the 3-D plot is that the v displacement is indeed greatest at the top and bottom corners of the border containing the crack tip and that the displacement gradually decreases as the distance along any plane parallel to x axis increases. This is the exact behaviour that can be expected.

The theoretical v displacement (Fig. 3(b)) agrees well with the experimental displacement. As in the experiment, v displacement is larger at the points closer to the tip and smaller at points away from it. However, the theoretical plots show

a much larger gradient near the tip predicting larger strain concentrations. It is possible that in the test specimen, strain energy near the tip dissipated into the growing plastic region thereby reducing strain concentration.

Horizontal displacement measures the amount of contraction in the tip area under the influence of a crack. It is expected to see a significant influence of tip on this profile as it was the case for v displacement. The experimental displacement profile is shown in Fig. 4(a) and it indeed shows a remarkable influence of the tip on this field. According to the plot, top and bottom corners of the border containing the tip receive the largest positive movement in x direction because crack lips force material near the tip to move in the positive direction. The displacement decreases as the tip is approached from either positive or negative y direction along this border. In part I of this study displacement profiles for wood without cracks were presented. It showed that in the absence of a crack the whole border was stationary (i.e. u = 0 along the border). Also, in the presence of a crack, all the points move in the positive direction, whereas, in the absence of a crack, whole displacement field is negative indicating contraction.

Fig. 4(b) shows the 3-D plot of the theoretical u displacement. There is remarkable similarity of displacement near the tip between the experimental and theoretical displacement plots. As in experimental data, u displacement along the border near the tip has the largest positive value. However, experimental results show a much greater drop in value in the 1.5 cm distance from the tip than the theoretical values which only display a small drop. Differences in the magnitude of the displacements can be partly attributed to the difference between average representation given by theory and a specific sample studied experimentally. Theoretical plot shows that u displacement is similar in magnitude to v displacements.

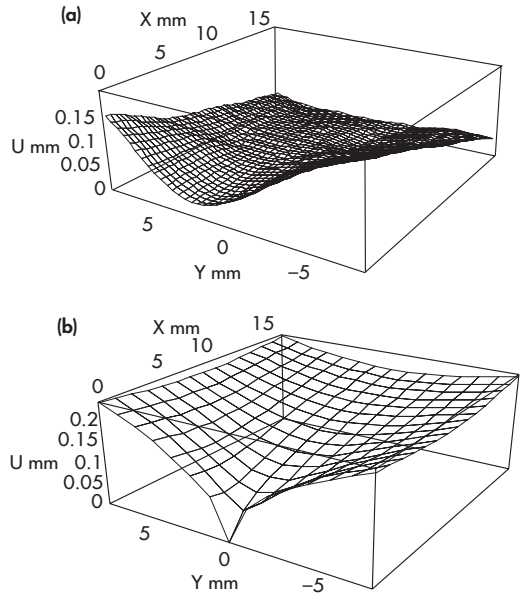

Fig. 4. Horizontal displacement fields for rubber with a crack. (a) experimental profile (b) theoretical profile.

4.2 Displacement Fields Near a Crack Tip for Mode-I Crack Parallel-to-Grain in wood

In this mode, crack is parallel-to-grain and therefore the loading is perpendicular to grain. Most of the load is transmitted through the lignin matrix. To obtain theoretical displacement fields, orthotropic fracture formulae (Equations (3) and (4)) were used with the following representative average properties for *Pinus radiata*: E_L = 8.0 GPa; E_R = 0.69 GPa; E_T = 0.41 GPa; G_{LT} = 0.62; υ_{TL} = 0.033; υ_{RL} = 0.041; υ_{RT} = 0.47.

Since average values are used in theoretical formulae, comparison can only be made in an average sense and more importance is placed on the trend and qualitative comparisons.

The experimental v displacement is displayed in Fig. 5(a) and corresponding theoretical plot is shown in Fig. 5(b). Some similarity in the two 3-D plots is immediately apparent, particularly the displacement gradient near the crack tip. Since load is applied perpendicular-to-grain, most of the v displacement can be attributed to that of the lignin matrix. The sharp gradient thus maybe

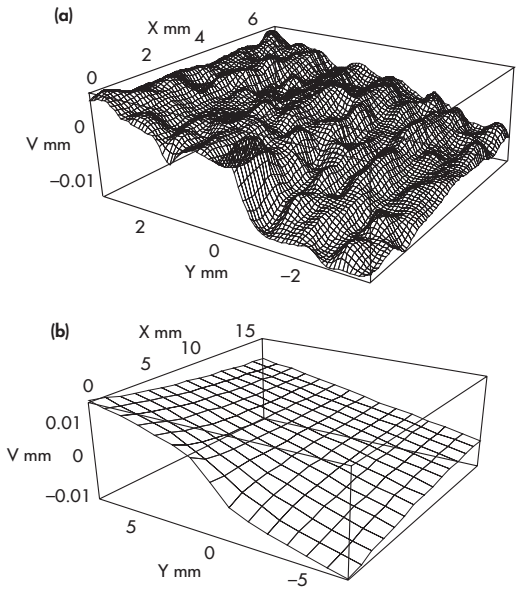

Fig. 5. Vertical displacement fields for wood with a crack parallel-to-grain. (a) experimental profile (b) theoretical profile.

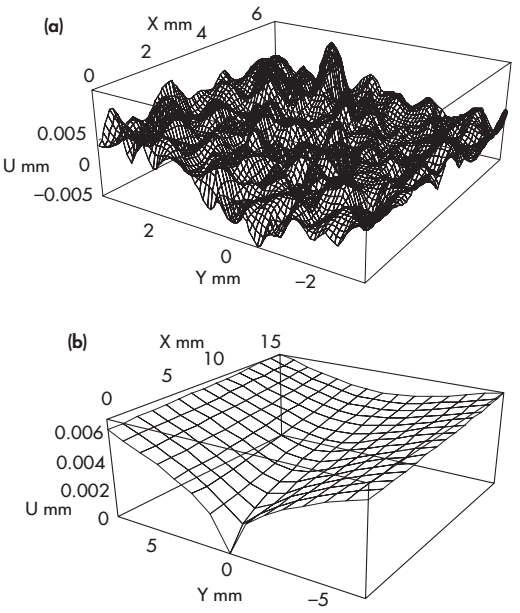

Fig. 6. Horizontal displacement fields for wood with a crack parallel-to-grain. (a) experimental profile (b) theoretical profile.

due to more flexible lignin, undergoing large relative displacements near the tip. The nature of displacement at the four corners are very similar and the overall trend is also the same despite the fluctuations of experimental values. The magnitude of displacement is also very similar in the experimental and theoretical plots. The most striking difference between the two 3-D plots is the wavy profile from the tested sample and the uniform profile from theory.

The u displacement measures horizontal displacement parallel-to-grain at points in front of the tip as a result of the applied stress perpendicular to the grain. Displacement profiles obtained from digital image correlation and orthotropic fracture theory are shown in Figs. 6(a) and 6(b), respectively. The theoretical u values as shown in the plot closely resembles that obtained for rubber (Fig. 4(b)). It is interesting to note that although the experimental profile is highly variable, a closer examination reveals a trend broadly similar to that depicted by theory. Theory assumes a purely orthotropic material whereas wood cannot be considered as truly orthotropic. Negative u displacement indicates the possible influence of mode II (shear) fracture in the vicinity of tip, which may be due to crack not being perfectly collinear with grain. It is apparent that the resemblance shown here is not as close as that between experimental and theoretical values for isotropic rubber. The magnitude of the experimental u values compares well with that of theory and the u displacement is much smaller than v displacement shown in Fig. 5(a). Note that u is measured along the direction of the tracheids. As already stated in Part 1 of this study, the profiles tend to be much noisier for the measurements made parallel-to-grain and a waviness propagates along the diagonal of the square area indicating a possible shear influence.

The magnitude of v and u displacements is within realistic ranges and compares well with theory. The experimental profiles are not as smooth and the effect is enhanced in the direction parallel-to-tracheids. The results strongly suggest the evidence of the influence of unique cellular structures on the crack tip displacements, which cannot be overlooked.

4.3 Displacement Profiles in Front of the Tip of a Crack Located Perpendicular-to-Grain in Wood

In this mode of loading, v displacement measures movement in the grain direction and u measures that across tracheids. For theoretical formulae, average material properties are the same as those used earlier.

The experimental and theoretical profiles of v displacement are shown in Figs. 7(a) and 7(b), respectively. The displacement pattern of the left (closer to tip), right, and bottom borders of the experimental plot shows that there is some resemblance in the overall behaviour to that predicted by theory. However, the sharp displacement gradient that is always present just above the tip in theoretical plots is absent in this experimental profile. Considering such high gradient shown in experimental profile for crack located parallel-to-grain discussed in the last section, the absence of such behaviour in the current profile must be due to the nature of elongation of tracheids invoking vertical slippage between tracheids. It appears thus that the displacement could be due to the combined effect of elongation and relative shearing. Another interesting point is that in the experimental field, crack tip influence is dominant throughout the area and diminishes slowly as the distance from the tip increases, whereas the theoretical profiles shows a much more localised effect of the tip influence which is almost absent in the far borders of the region. The overall displacement values for the two plots are comparable. Usual wavy bands that have become a common feature in the discussion so far are apparent here as well along with the 45° angular wave pattern. We have already established that the displacement profiles parallel to tracheids are much coarser than that perpendicular to tracheids. Comparison of the two contour plots show how theory resembles actual behaviour but misses the details peculiar to the features of a real material.

The measured displacement across the grain (u) is mainly due to lignin. The experimental and theoretical profiles are shown in Figs. 8(a) and 8(b), respectively. Once again, some similarities and dissimilarities are apparent from the plots. For example, for negative y co-ordinates, the

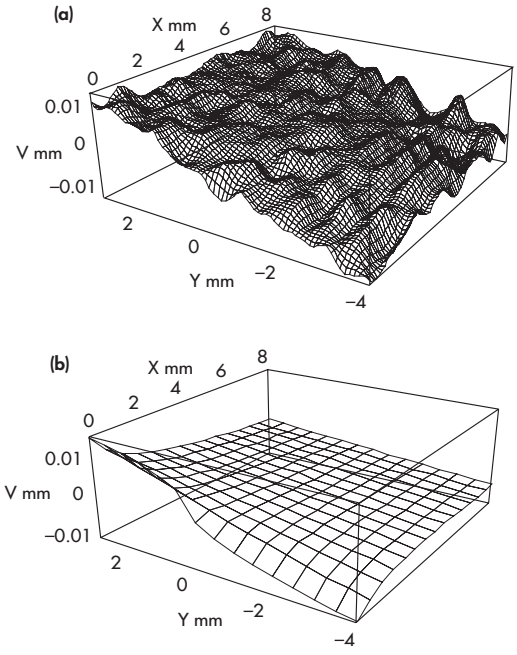

Fig. 7. Vertical displacement fields for wood with a crack perpendicular-to-grain. (a) experimental profile (b) theoretical profile.

experimental profile closely resembles that of the theoretical profile; however the top corner of the left border (closer to tip) undergoes a movement in the negative x direction in the experimental profile. This can happen due to mode-II shear influence which acts in the direction of negative x axis. A major feature of both plots is that u displacement is much greater than the vertical v displacement when measured relative to the tip. This was not the case for crack parallel to grain. Larger u values compared to those of v must be due to deformation of the lignin matrix under the influence of crack tip stress field. As found for the other experimental profiles, shear influence is clearly seen here too. The theoretical plot compares well with the experimental profile to a large extent but experimental profiles demonstrate complexities associated with real material behaviour, which cannot be fully captured by theory.

Owing to the nature of the behaviour of tracheids, a sharp gradient near the tip is not obtained in experimentally tested specimens with a

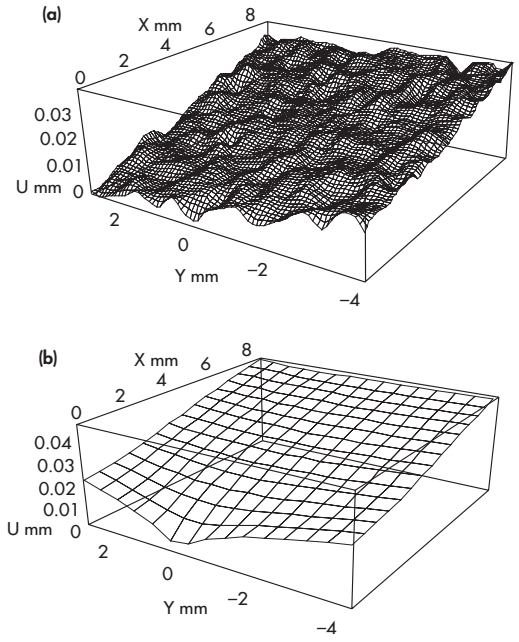

Fig. 8. Horizontal displacement fields for wood with a crack perpendicular-to-grain. (a) experimental profile (b) theoretical profile.

crack loaded parallel-to-grain as predicted by theory. It can be said that some general features depicted by the theory are followed by the tested sample. However, experimental profiles are more complex as a result of the material not being truly orthotropic and the cellular structure that appears to produce mode-II type influence on u displacement, vertical slippage, and significant internal shear. Crack tip has a prominent influence on the horizontal displacement near the tip.

5 Mixed-mode Fracture

In mixed-mode fracture, both opening and shearing modes influence crack tip displacement fields; therefore v and u displacements are the combined total displacements due to both modes in respective directions. Crack was parallel-to-grain in all mixed mode specimens and experimental results are presented for a 9 mm × 9 mm area near the tip as shown in Fig. 2(b) which also shows the convention of the co-ordinate system. Specifically, crack tip is stationary with co-ordinates (0,0), x axis lies in the crack plane, and y axis is perpendicular to it. All displacements are presented relative to the tip.

The theoretical displacements were also obtained from orthotropic fracture theory. Here displacement components for mode-I and II were combined to obtain total u and v using Equations (5) and (6), respectively. Material properties are the same as the average properties used previously. K_I and K_{II} values were determined from

$$K_I = Y_1 \sigma \left(\sqrt{\pi a}\right) \mathrm{Sin}^2 \alpha \tag{7}$$

$$K_{II} = Y_2 \sigma \left(\sqrt{\pi a}\right) \mathrm{Sin}\alpha \,\mathrm{Cos}\alpha \tag{8}$$

where α is the crack angle with respect to the load axis ((Fig. 2(b)), a is the crack length, σ is the applied remote stress, Y_1 is the mode I correction factor (1.2978), Y_2 is the mode II correction factor (1.0) (Tada et al. 1985).

Before proceeding to the discussion of results, a look ahead at what can be expected will aid the discussion. In mixed-mode, the remote applied stress (σ) can be resolved into normal (σ_I) and shear (τ_{II}) stress components (i.e. mode I and mode II stress components). These are:

$\sigma_I = \sigma\ \mathrm{Sin}^2\alpha$; $\tau_{II} = \sigma\ \mathrm{Sin}\ \alpha\,\mathrm{Cos}\alpha$;
For $\alpha = 30°$, $\sigma_I = 0.25\sigma$, $\tau_{II} = 0.433\sigma$;
For $\alpha = 45°$, $\sigma_I = \tau_{II} = 0.5\sigma$;
For $\alpha = 60°$, $\sigma_I = 0.75\sigma$, $\tau_{II} = 0.433\sigma$.

The mode II shear stress is relatively constant for the three angles tested with 45° angle showing the highest shear stress. In contrast, influence of mode I fracture increases with crack angle. Therefore, 60° angle must show the largest combined total v displacement followed by 45° and 30° must show the least. As for u displacement, mode I component should increase with crack angle owing to increased normal stress and the mode II influence is relatively constant for the angles tested due to similar shear stresses for the three angles. With the aid of the above description, the following experimental and theoretical displacement profiles can be studied to understand the crack tip behaviour under mixed-mode loading and the relevance of the theory to predict the same.

5.1 30° Crack Angle

Fig. 9(a) shows the experimental 3-D plot for v displacement and Figs. 9(b), (c), and (d) show theoretical mode-I, mode-II, and combined total v displacement respectively. At this angle shear stress is larger than normal stress and therefore, a dominant mode II influence can be expected. Theoretical plots in Fig. 9(b) and (d) reveal how mode-II v displacement component alters the already familiar mode I displacement profile to produce the combined total displacement for a truly orthotropic material. Specifically, there is a relatively large negative mode-II v displacement away from tip which decreases towards the tip. The basic mode-II influence is a uniformly varying downward pull of the displacement profile resulting in much increased negative total displacements for negative y values, particularly in the bottom right-hand region in the analyzed area. A variation of this interplay is expected as the crack angle increases. In the experimental plot, the overall pattern depicted by theory is maintained although the plot is not smooth and the overall magnitude of displacement also compares reasonably well. Although there is a sharp displacement gradient near the tip as predicted by theory, the displacement along the border closer to the tip not as smooth as in theory. This gradient can be attributed to mode-I v displacement (Fig. 9(b)).

Due to the larger shear stress component, mode-II influence must be more prominent here than that for v. Fig. 10(a) shows the experimental displacement plot and Figs. 10(b), (c) and (d) show theoretical mode-I, mode-II, and combined total displacements, respectively. According to theory, mode-I u displacement is all positive, whereas, mode-II contribution introduces a crack tip gradient as well as positive and negative displacements above and below x axis respectively. As expected mode-II u displacement is much greater than mode-I u displacement component. The theoretical combined total displacement plot (Fig. 10(d)) reveals a very strong influence of mode-II displacement in the region below x axis. Except for the top left hand corner, the experimental profile vaguely follows the general trend

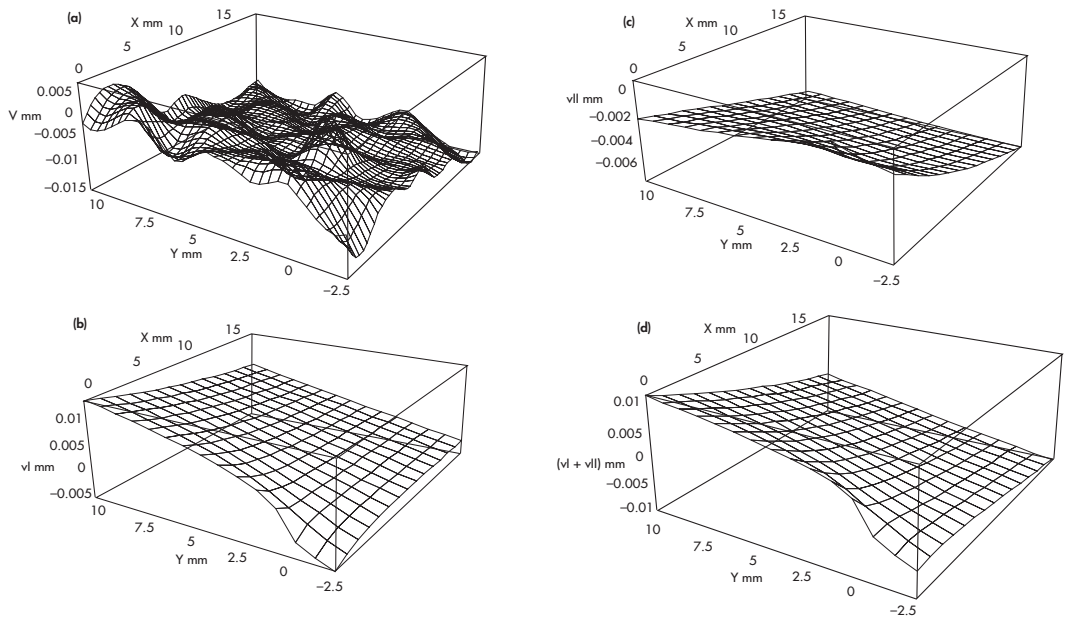

Fig. 9. Vertical displacement fields for 30° crack angle to load in wood with crack parallel-to-grain. (a) experimental profile (b) theoretical mode-I component (c) theoretical mode-II component and (d) combined mode-I and mode-II (total) theoretical profile.

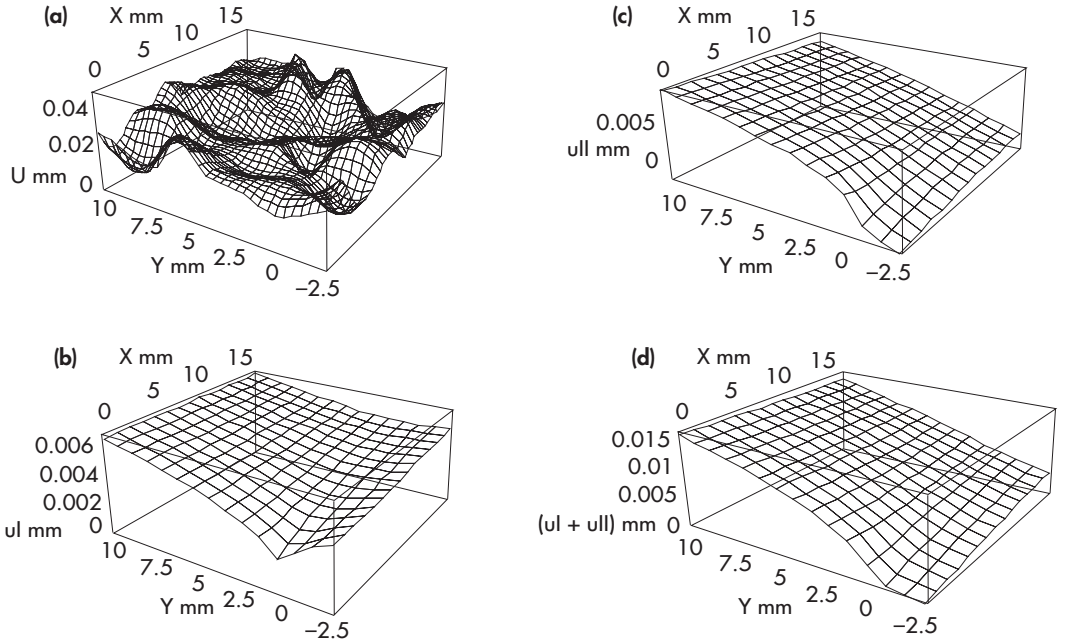

Fig. 10. Horizontal displacement fields for 30° crack angle to load in wood with crack parallel-to-grain. (a) experimental profile (b) theoretical mode-I component (c) theoretical mode-II component and (d) combined mode-I and mode-II (total) theoretical profile.

depicted by theory; however, it appears that the severe distortion present in the plot makes it deviate from the predicted pattern. Note that the displacement is parallel to tracheids. In both plots all u displacements are positive; however, the experimental values are larger than predicted, which have been accentuated by peaks in the plot. The u values exceed v displacement in both theoretical and experimental plots.

5.2 45° Crack Angle

At this angle normal and shear stress components are equal. Fig. 11(a) displays experimental displacement profile and Fig. 11(b) shows theoretical combined total v displacement, respectively. According to theory, both mode-I and II components (not shown here) are higher than those for 30° angle and the total displacement is predominantly due to mode-I contribution. The effect of mode-II is to pull the displacement down in the negative direction. However, the overall effect of this is smaller compared to that for 30° crack angle showing the effect of increased normal stress. Also, there is a much greater resemblance between experimental and theoretical plots for 45° crack angle compared to 30° angle. Experimental plot also reveals a steep displacement gradient near the tip as predicted by theory. In this case, the overall pattern and magnitude of displacements are similar in experiments and theory. As expected, v displacement for 45° crack angle is greater than that for 30° angle as can be seen from Figs. 11(a) and 9(a).

The experimental u displacement profile is given in Fig. 12(a) and theoretical combined total displacement plot is shown in Fig. 12(b). According to theory, mode-I displacement has considerably increased compared to that for 30° crack angle and mode-II components have also slightly increased (not shown here). The combined displacement plot reveals that the overall effect of mode-II is less than that for 30° angle owing to the influence of the larger normal stress.

Much smoother experimental u displacement

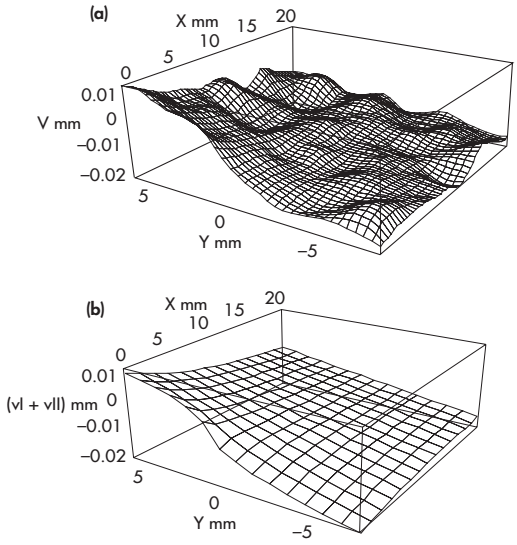

Fig. 11. Vertical displacement fields for 45° crack angle to load in wood with crack parallel-to-grain. (a) experimental profile (b) theoretical profile.

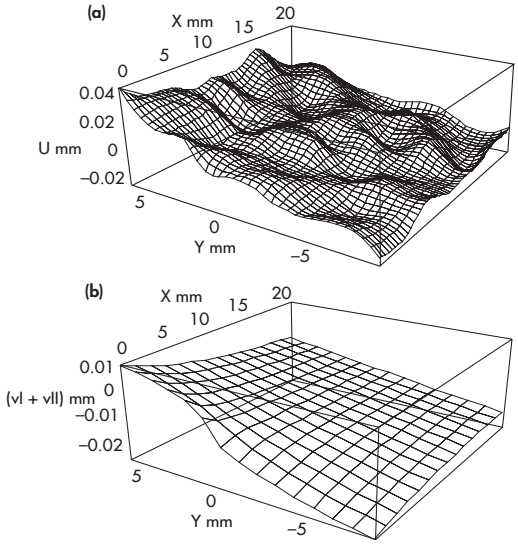

Fig. 12. Horizontal displacement fields for 45° crack angle to load in wood with crack parallel-to-grain. (a) experimental profile (b) theoretical profile.

is evident from Fig. 12(a) where overall displacement is greater than those for 30° angle, that confirms the expected trend. Comparison of the experimental results with the theoretical profile indicates a general agreement in the trend above x-axis but below x-axis u is negative for the most part in experimental plot. The u displacement below the x-axis is positive in theoretical plots. Recall that negative u displacement below the x-axis comes from mode II contribution. Thus, experimental results show a stronger influence of mode II than indicated by theory. As for 30° angle, experimental displacements are larger than predicted.

5.3 60° Crack Angle

At 60° normal stress component is the largest for the angles tested. Here $\sigma_I = 0.75\sigma$ and $\tau_{II} = 0.433\sigma$. The experimental profile for v displacement is displayed in Fig. 13(a) and theoretical total v displacement is shown in Fig. 13(b). As can be expected, theory indicates a much larger mode-I contribution than mode-II (not shown here) and reveals the largest overall v displacement for this angle compared to 45° and 30° crack angles. The mode-II component is similar to that for 45° angle. The increased mode-I contribution diminishes the effect of mode-II even more so than that for 45° angle. Experimental profile more resembles theory than that for the other two angles and it is interesting to note that the degree of disturbance in the experimental plots decreases as the crack angle increases. The theoretical plot captures the most important features of the experimental profile including the steep gradient at the tip and the overall magnitudes in the two plots compare well. One noticeable feature though is that for 60° angle crack tip influence diminishes much more slowly towards the back border in the experimental results compared to the theoretical profile.

Owing to high normal stress, u displacement for 60° is expected to be larger than that for 45° and 30°. Fig. 14(a) shows the experimental plot which indeed shows that the displacement is almost twice as large as that for 30° and roughly about 50 % greater than that for 45° angle. This plot indicates that the u displacement plots also

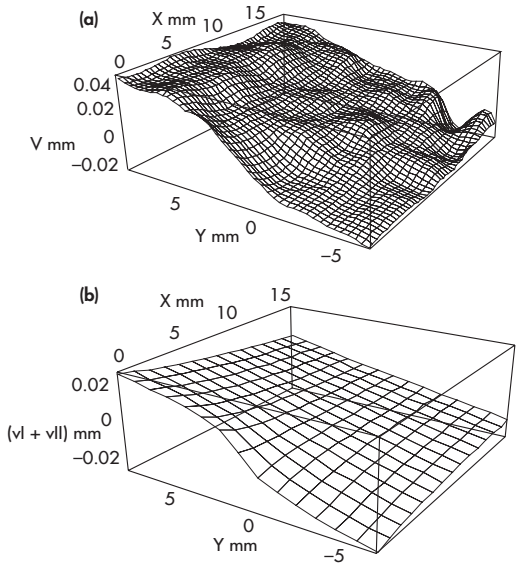

Fig. 13. Vertical displacement fields for 60° crack angle to load in wood with crack parallel-to-grain. (a) experimental profile (b) theoretical profile.

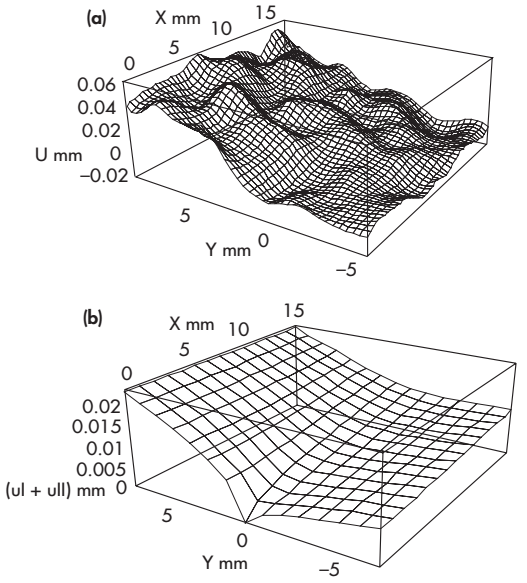

Fig. 14. Horizontal displacement fields for 60° crack angle to load in wood with crack parallel-to-grain. (a) experimental profile (b) theoretical profile.

get smoother as the crack angle increases. Fig. 14(b) shows the combined total u displacement. According to theory, mode-I component has increased but mode-II component has stayed almost at the same level as that for 45° angle (plots not shown here). The overall effect is an increased total displacement compared to the other two angles. Fig. 14(b) clearly shows the diminished mode-II influence owing to high mode-I contribution. The experimental plot more resembles theory than those for the other two angles. As shown earlier, experiments reveal a larger mode-II contribution than predicted leading to negative u values below x axis whereas in theory u is positive. Once again, experimental displacements are larger than predicted values.

6 Summary and Conclusions

Near tip displacements were obtained for cracked rubber and wood- with a crack parallel- and perpendicular-to-grain, and an inclined crack located along the grain of wood but loaded at 30°, 45°, and 60° to the crack plane using digital image correlation method. The displacement profiles thus obtained revealed intricate details of the mechanisms of load transfer in isotropic rubber and anisotropic wood with a crack confirming that the digital image correlation is a useful method for detailed analysis of crack tip displacements. For cracked rubber and wood members, theoretical displacements were also computed and compared with experimental values.

The experimental plots for mode-I fracture clearly showed the remarkable influence of the tip on both u and v displacements; particularly the major changes in the u displacement profile compared to that without a crack. Trend and magnitude of displacement in theoretical and experimental plots for wood compared well. As found for uncracked wood specimens in Part 1 of this study, displacements parallel-to-tracheids in cracked members produce complex displacement profile subjected to slippage and distorted by internal shear stress, whereas, displacement perpendicular-to-tracheids produce comparatively smoother profiles.

In mixed mode fracture, experimental plots revealed the influence of crack angle very clearly. For example, as crack angle increases, both u and v displacement components increase and plots revealed the combined influence of mode-I and mode-II. Theoretical and experimental v displacement profiles compare well. The u displacement profiles showed some agreement but experiments indicated a larger mode-II influence than predicted and experimental u values are also higher than predicted.

In conclusion, orthotropic fracture theory is useful for crack tip analysis of wood. It gives good predictions for perpendicular-to-grain displacements. It captures the overall trend in the displacement parallel-to-grain but is unable to capture the total complexity of the behaviour patterns associated with tracheids and internal shear.

References

Durig, B., Zhang, F., McNeill, S.R., Chao, Y.J. & Peters, W.H. 1991. A study of mixed mode fracture by Photoelasticity and digital image analysis. Optics and Laser Engineering 14: 26–34.

Irwin, G.R. 1957. Analysis of stresses and strains near the end of a crack traversing a plate. Journal of Applied Mechanics 24: 361–364.

Wolfram Research. 1997. Mathematica version 3.0.

McNeill, S.R., Peters, W.H. & Sutton, M.A. 1987. Estimation of stress intensity factor by digital image correlation. Engineering Fracture Mechanics 28(1): 101–112.

Samarasinghe, S., Kulasiri, G.D. & Nicolle, K. 1996. Study of mode-I and mixed-mode fracture in wood using digital image correlation method. Proceedings of the International Wood Engineering Conference, New Orleans, USA. 4: 144–151.

— & Kulasiri, G.D. 1998. Investigation of stress intensity factors of wood using image processing and orthotropic fracture theory. Proceedings of the 12th Engineering Mechanics Conference (ASCE), La Jolla, San Deigo, USA. (in CD Rom)

— & Kulasiri, G.D. 1999. Fracture toughness of wood based on experimental near-tip displacement fields and orthotropic fracture theory. Proceedings of the Pacific Timber Engineering Conference, Rotorua, New Zealand.

Sih, G.C., Paris, P.C. & Irwin, G.R. 1965. On cracks in rectilinearly anisotropic bodies. International Journal of Fracture Mechanics 1: 189–203.

Tada, H., Paris, P.C. & Irwin, G.R. 1985. The stress analysis of cracks handbook. 2nd Edition, Paris Productions, Inc., St. Louis.

Vic-2D. Version 2.1. 1998. Digital Image Correlation, Cimpiter, Inc. USA.

Westergaard, H.M. 1939. Bearing pressure and cracks. Journal of Applied Mechanics 6: 49–53.

Williams, M.L. 1957. On the stress distribution at the base of a stationary crack. Journal of Applied Mechanics 24: 109–114.

Total of 12 references